

Biomechanical Properties of Bruch's Membrane–Choroid Complex and Their Influence on Optic Nerve Head Biomechanics

Xiaofei Wang,¹ Clarence Ken Guan Teoh,¹ Anita S. Y. Chan,^{2,3} Sathiyar Thangarajoo,¹ Jost B. Jonas,^{4,5} and Michaël J. A. Girard^{1,2}

¹Ophthalmic Engineering & Innovation Laboratory, Department of Biomedical Engineering, Faculty of Engineering, National University of Singapore, Singapore

²Translational Ophthalmic Pathology, Singapore Eye Research Institute, Ophthalmic Pathology Service, Singapore National Eye Centre, Singapore

³Duke-National University of Singapore Medical School, Singapore

⁴Department of Ophthalmology, Medical Faculty Mannheim of the Ruprecht-Karls-University, Heidelberg, Germany

⁵Beijing Institute of Ophthalmology, Beijing Tongren Eye Centre, Beijing Tongren Hospital, Capital Medical University, and Beijing Key Laboratory of Ophthalmology and Visual Sciences, Beijing, China

Correspondence: Michaël J. A. Girard, Ophthalmic Engineering & Innovation Laboratory, Department of Biomedical Engineering, National University of Singapore, Engineering Block 4, #04-8, 4 Engineering Drive 3, Singapore 117583; mgirard@nus.edu.sg.

Submitted: April 18, 2017

Accepted: April 19, 2018

Citation: Wang X, Teoh CKG, Chan ASY, Thangarajoo S, Jonas JB, Girard MJA. Biomechanical properties of Bruch's membrane–choroid complex and their influence on optic nerve head biomechanics. *Invest Ophthalmol Vis Sci.* 2018;59:2808–2817. <https://doi.org/10.1167/iovs.17-22069>

PURPOSE. The purpose of this study was to measure the rupture pressure and the biomechanical properties of porcine Bruch's membrane (BM)–choroid complex (BMCC) and the influences of BM on optic nerve head (ONH) tissues.

METHODS. The biomechanical properties of BMCC were extracted through uniaxial tensile tests of 10 BMCC specimens from 10 porcine eyes; the rupture pressures of BMCC were measured through burst tests of 20 porcine eyes; and the influence of BM on IOP-induced ONH deformations were investigated using finite element (FE) analysis.

RESULTS. Uniaxial experimental results showed that the average elastic (tangent) moduli of BMCC samples at 0% and 5% strain were 1.60 ± 0.81 and 2.44 ± 1.02 MPa, respectively. Burst tests showed that, on average, BMCC could sustain an IOP of 82 mm Hg before rupture. FE simulation results predicted that, under elevated IOP, prelamina tissue strains increased with increasing BM stiffness. On the contrary, lamina cribrosa strains showed an opposite trend but the effects were small.

CONCLUSIONS. BMCC stiffness is comparable or higher than those of other ocular tissues and can sustain a relatively high pressure before rupture. Additionally, BM may have a nonnegligible influence on IOP-induced ONH deformations.

Keywords: Bruch's membrane, biomechanical properties, rupture pressure, intraocular pressure, finite element analysis

Bruch's membrane (BM) is a membrane located in between the RPE and the choroid. BM forms part of the eye wall for more than two thirds of the surface of the eye. Including the basal membrane of the RPE and choriocapillaris, BM plays an important role in preserving the blood–retina barrier and in keeping the retinal interstitial space mostly fluid free.¹ Structural and biomechanical changes in BM may be linked with macular disorders including AMD.² Anatomical changes of BM in association with changes in the RPE and choriocapillaris in the vicinity of the optic nerve head (ONH) are associated with the formation of peripapillary zones, which have been categorized into alpha zone (presence of BM with irregular RPE), beta zone (absence of RPE and presence of BM), and gamma zone (absence of BM).³ These zones have been well documented in glaucoma and highly myopic patients,^{3,4} and their developments may be linked to changes in IOP,^{5–7} eye movements, and other mechanisms.^{8,9} In glaucoma, the size of peripapillary beta zone was correlated with progression of glaucomatous visual field loss,¹⁰ whereas the gamma zone was correlated with an increase of the optic disc–fovea distance and

with an axial elongation–associated vertical optic disc rotation around the vertical axis.¹¹ An active force generated by BM in the midperiphery of the fundus has recently been hypothesized to play a role in axial elongation in the process of emmetropization/myopization.¹²

Knowledge of the biomechanical properties of BM may be helpful to improve our understanding of the basic physiology of the eye and its pathophysiology including the development of myopia, glaucoma, AMD, and the development of peripapillary atrophy. Surprisingly, little research has been performed to characterize the biomechanical properties of BM. Direct measurement of the BM stiffness is currently hindered by difficulties in isolating BM. Therefore, studying the BM–choroid complex (BMCC) may give us an insight into the BM properties. Previous studies have investigated the pressure–deformation relationship¹³ and the elastic modulus of BMCC.¹⁴ However, these studies either used a linear elastic material model (unsuitable for collagenous membranes)¹⁴ or examined the pressure–deformation relationships using unconventional engineering units.¹³ Furthermore, no study has yet investigated the



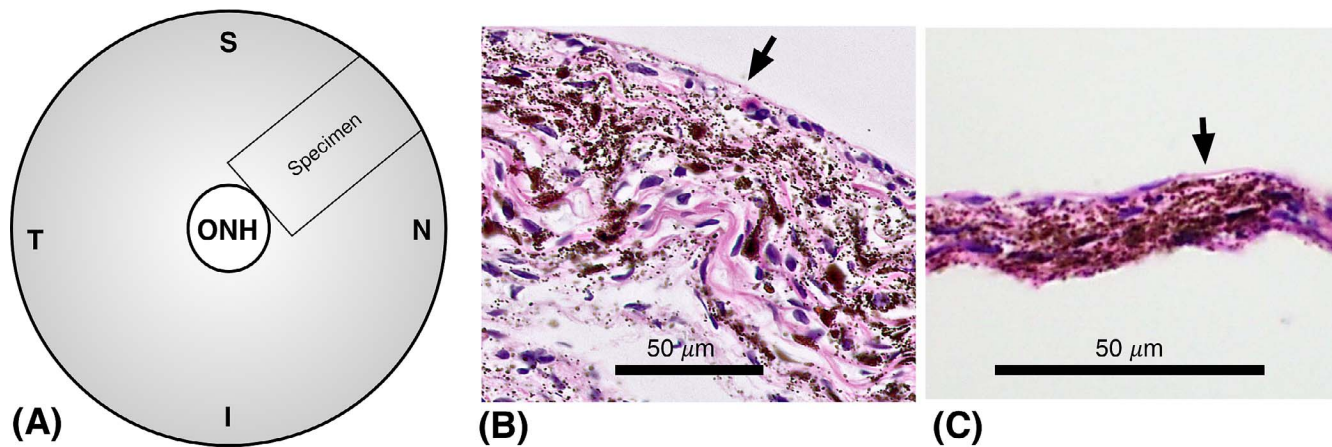


FIGURE 1. (A) Posterior view of a porcine eye showing the location of a BM-choroid specimen for tensile testing. (B) Histologic image of a full-thickness BM-choroid complex sample that was dissected away from the sclera. The thicknesses of these samples were approximately 80 μm as measured from 10 samples using OCT. (C) Histologic image of a final specimen in which a large portion of the choroid was removed. Hematoxylin and eosin stain was used in the histology. Arrows indicate BM.

mechanical contribution of BM to IOP-induced ONH deformations, although BM is connected with the ONH via the peripapillary choroidal border tissue of Jacoby and BM exhibits structural changes in the peripapillary region both in myopia and glaucoma. We conducted this experimental study to more comprehensively examine the biomechanical properties including the rupture pressure of BMCC and, using finite element (FE) analysis, to investigate the mechanical role of BM in eyes with elevated IOP.

METHODS

The biomechanical properties of BMCC were measured through uniaxial tensile testing of BMCC tissue strips. Note that in the uniaxial tensile test, we removed a large portion of the choroid from the specimen to reduce its thickness to $\sim 20 \mu\text{m}$, which is different from two previous studies using full-thickness BMCC. The rupture pressure of BMCC was assessed through burst testing. We then built FE models of the eye that incorporated BM geometry and biomechanical properties (as assessed experimentally). Finally, using such models, we estimated the contribution of BM to ONH deformations following an acute elevation of IOP.

All study tissues were obtained from porcine eyes. Ten eyes were used for the uniaxial tensile test, and the remaining eyes were used for testing the strength of BM under elevated IOP. The eyes were obtained from a local slaughterhouse in Singapore within 24 hours postmortem. Pigs were 6 months old when killed.

Uniaxial Tensile Tests of BMCC

Sample Preparation. For each eye, the anterior chamber, vitreous, and retina were removed, and a scleral strip (with BM and the choroid attached to it) was dissected away from the eye globe. Each strip was aligned along the radial direction in the supero-temporal quadrant (from the ONH to the equator; Fig. 1A) with a length of about 15 mm and a width of about 5 mm. Then, the BMCC was gently dissected away from the sclera using a forceps under a dissecting microscope. Special care was taken in regions where the choroid was tightly attached to the sclera by the vortex veins. The samples obtained from this step were full-thickness BMCCs as illustrated by histology (Fig. 1B) and were on average 80 μm in thickness as measured from 10 samples using a custom

optical coherence tomography (OCT) system (pixel resolution: 1 μm). To further isolate BM, we dissected away part of the choroid in the central region, and then we gently brushed off the specimen with a cotton swab. Through this step, a large portion of the choroid was removed; however, as the choriocapillaris is firmly connected to BM, we were unable to completely remove the choroid from BM without damaging the sample. Figure 1C shows a typical BMCC specimen (used for uniaxial testing) that includes both BM and a small portion of the choroid. Specimens were on average $21 \pm 4.9 \mu\text{m}$ as measured by the custom OCT system and were examined through a microscope (Olympus IX71; Olympus, Tokyo, Japan) to assess their mechanical integrity. Samples that we damaged during this dissection procedure were discarded. Throughout the dissection process, all samples were kept hydrated with PBS.

Uniaxial Tensile Test. Each BMCC specimen was mounted between the two grips of a uniaxial tensile tester (Instron-5848; Instron, Inc., Norwood, MA, USA). The length (grip-to-grip distance) and width of each sample were then measured using a Vernier caliper (resolution: 0.01 mm). The thickness of each sample was measured using a custom OCT system (pixel resolution: 1 μm) around 30 minutes before the uniaxial test. A preload of 0.01 N was applied to the specimen, and zero displacement was defined after this load. Next the specimen was subjected to a uniaxial preconditioning in tension,¹⁵ consisting of 10 cycles from 0% to a maximum of 1% strain at a rate of 1%/s. Our preconditioning protocol was validated (through convergence of stress/strain curves) and is similar to that in our prior scleral experiments.^{15,16} The specimen was allowed to recover for 5 minutes, and then a 1% per second strain ramp to a stretch ratio of 1.2 or more was applied to the tissue. This strain rate was used based on a previous study on scleral biomechanical properties.¹⁵ During the 5-minute recovery period, we sprayed PBS onto the sample every minute to ensure it remained hydrated. The time span of the uniaxial tensile test was on average 20 seconds. During this period, we believe it is safe to assume that the samples remained hydrated. Forces and deformations (grip-to-grip distance changes) were recorded by the uniaxial tensile tester. The displacement of the uniaxial tester is accurate to 1 μm . The typical force generated by the specimen at the end of uniaxial testing was approximately 0.2 N. The load cell has a capacity of 10 N and is accurate to 0.5% at 1/500 maximum load. Before each experiment, the load cell was calibrated with

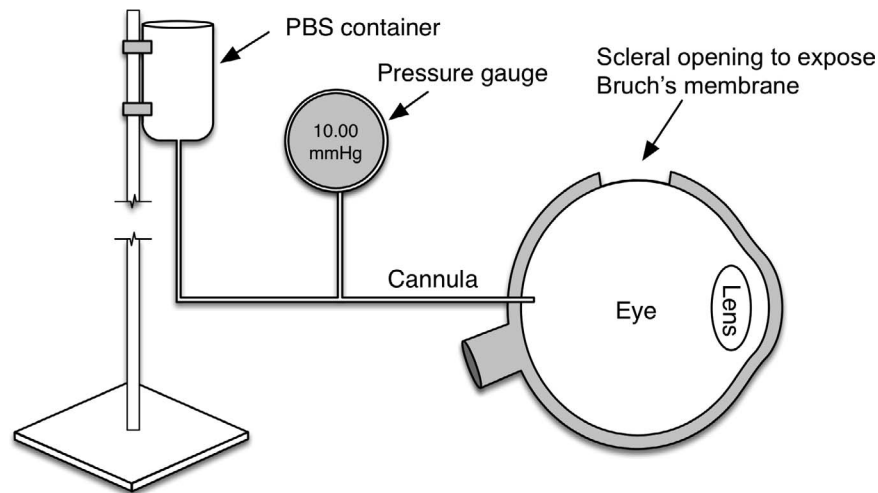


FIGURE 2. Schematic of the burst test setup.

the Bluehill software (Instron, Inc.). The accuracy of the load cell was also verified by using standard weights.

Extraction of Biomechanical Properties. To extract the mechanical properties of the samples, we assumed a homogeneous stress/strain field in the specimen. For each specimen, the experimental force-stretch curve was fitted to a Yeoh model using a least squares curve-fitting algorithm, lsqcurvefit, in Matlab (Version 2015a; Mathworks, Inc., Natick, MA, USA).¹⁷ The strain energy function of the Yeoh model can be found in the Supplementary Material. We used two hyperelastic constants (c_1 , c_2) to describe the stress-strain relationships

for this material model, which can be derived from the experimental data presented above.

Rupture Pressure of BMCC Under Elevated IOP

Tissue Preparation. All 20 eyes were cleaned of extra-orbital tissues such as muscles and fat. A square patch excision of scleral tissue and choroid was made to expose the underlying BMCC (Figs. 2, 3A). The BMCC and retina remained intact to bear the subsequent IOP loading. To ensure consistency across experiments, the same square patch area

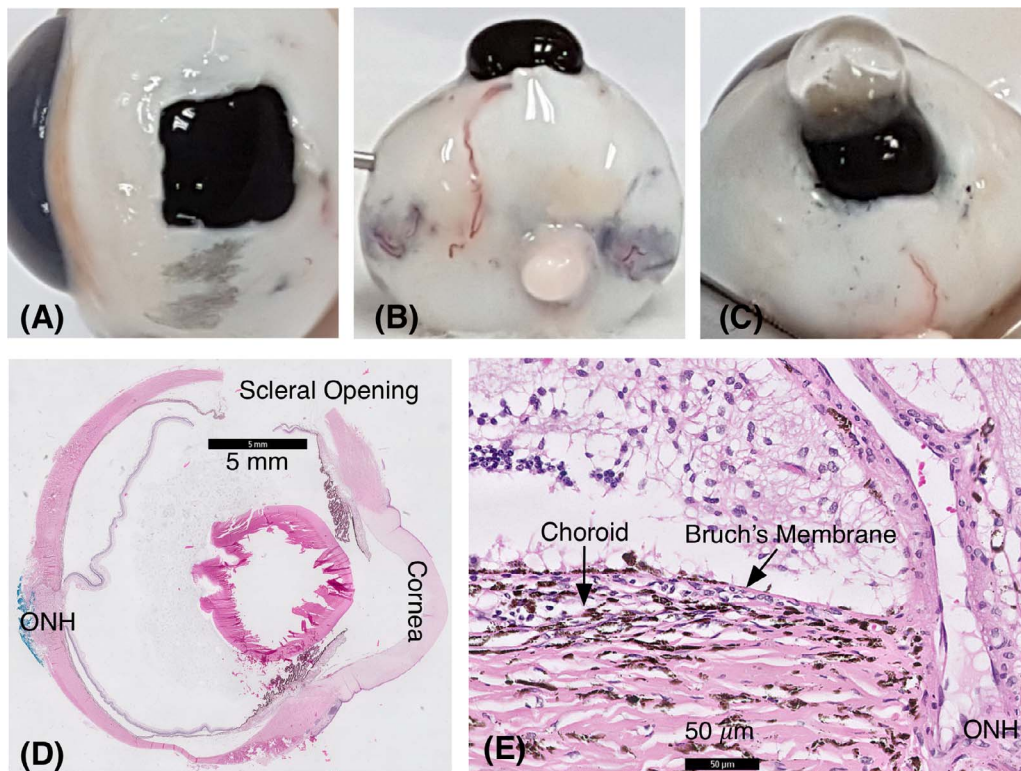


FIGURE 3. (A) Photograph of the eye with a 7 × 7-mm square section of the sclera and choroid removed to expose the underlying BM. (B) Photographs of the pressurized eye with the exposed bulging BM. (C) Vitreous leakage indicating BM rupture. (D) Histologic section of an eye globe after a burst experiment. There was no detachment of BM around the ora serrata and around the ONH even after rupture in the equatorial region (scleral opening). (E) A zoomed image of the ONH region demonstrating the mechanical integrity of BM.

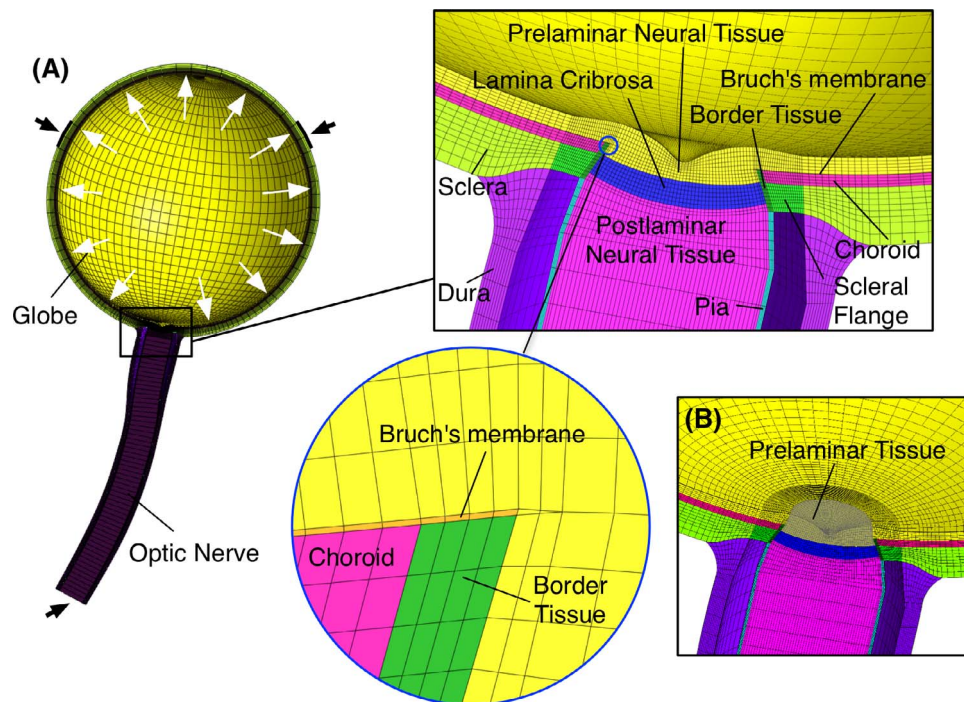


FIGURE 4. (A) Geometry and mesh of the FE model with BM. Detailed ONH structures were included (sclera, LC, neural tissue, pia, dura, choroid, and BM) using average measurements from the literature. (B) A zoomed image of the ONH region showing the ONH prelaminar tissue. *Black arrows* indicate fixed faces or elements. *White arrows* indicate IOP loading of 50 mm Hg.

(approximately 7×7 mm) of scleral tissue was removed in all eyes and in the same location (superior equatorial region). After removing the scleral and choroid, inspection was performed to ensure that there was no damage to the exposed BMCC for all eyes. The eye was discarded if any damage to BMCC was observed.

IOP Elevation. A pressure column containing PBS was used to inflate each eye globe through a 28-gauge needle (outer diameter, 0.36 mm) inserted into the vitreous chamber at the equator (Fig. 3B). A digital pressure gauge (XP2i Digital Test Gauge; Crystal Engineering, Berwyn, PA, USA) connected to the needle was used to monitor the pressure that was applied to the globe. Prior to burst testing, each eye was pressurized to 15 mm Hg for 30 minutes to allow for the ocular tissues to reach biomechanical equilibrium. This pressure level was chosen as it is a typical physiologic IOP level in porcine eyes *in vivo*.¹⁸ Next, the pressure was increased by manually raising the height of the PBS column. We used a pressure increment of 1 mm Hg for each step, and the pressure was maintained constant for 1 minute before the next pressure increment. This process was repeated until we observed BMCC rupture. Figure 3B shows the considerable bulging of BM (that has not yet ruptured) under a pressure of 60 mm Hg.

Rupture Criterion. We assumed that mechanical failure of BMCC occurred when we observed vitreous humor leakage through the dissected square patch area, as shown in Figure 3C. The measurement displayed on the pressure gauge when this incidence occurred was taken as the pressure required to induce mechanical failure of BMCC. All eyes were subsequently dissected to ensure that BM did not detach in the ora serrata and ONH regions.

Histologic Processing

We performed histology to confirm that (1) the uniaxial tensile specimens contained BM and only a relatively small portion of

the choroid only and (2) BM did not detach in the ora serrata and the ONH regions following burst testing.

To this end, four BMCC specimens were removed and immediately fixed in 10% formalin. Following burst testing, one eye globe was also immersion fixed for 24 hours in the same solution. All specimens were transported to the diagnostic histopathology laboratory at the Singapore General Hospital, and then embedded in paraffin and processed according to established protocols.¹⁹ Briefly, both BMCC and eye globe specimens were sectioned to generate 4- μ m sections that were deparaffinized, stained with hematoxylin and eosin using an autostainer (Leica Autostainer XL; Leica Instrument, Nussloch, Germany), and then coverslipped.

Use FE to Study the Structural Role of BM

Geometry of the FE Models. The geometry of the FE model was modified from our previous studies.^{9,20} The models included the corneo-scleral shell, peripapillary sclera, scleral flange, retina, choroid, prelaminar neural tissue, lamina cribrosa (LC), postlaminar neural tissue, pia, and dura. Detailed geometric parameters can be found in the recent literature.^{9,20} In addition, we included the border tissues²¹ of the choroid (Jacoby) and of the scleral flange (Elschnig) into the models as BM forces may be directly transmitted to the ONH through these tissues. The thickness of the border tissues was set as 0.06 mm.²¹ The thickness of the choroid and of BM were taken as 134²² and 5 μ m,²³ respectively. The reconstructed model was discretized into a hexahedron-dominant mesh with 154,628 eight-node hexahedra and 3672 six-node pentahedra elements. All tissues were bonded together if they shared nodes at tissue boundaries (Fig. 4). Finally, the mesh density for the FE model was numerically validated through a convergence test (Supplementary Material).

Biomechanical Properties. In the baseline model, BM was described as a hyperelastic Yeoh material that was given

TABLE 1. Tissue Biomechanical Properties Used for the Baseline Model

Tissue	Constitutive Model	Biomechanical Properties	References
Sclera	Mooney-Rivlin Von Mises distributed fibers	c1 = 0.063 MPa c3 = 0.0194 MPa c4 = 273 kf = 2 (scleral flange) kf = 0 (other region of sclera) θp: preferred fiber orientations*	Girard et al. ⁴⁴
BM	Yeoh model	c1 = 0.27 MPa c2 = 2.65 MPa	This study
Choroid	Isotropic elastic	Elastic modulus = 0.6 MPa Poisson's ratio = 0.49	Friberg and Lace ¹⁴
Dura	Yeoh model	c1 = 0.1707 MPa c2 = 4.2109 MPa c3 = -4.9742 MPa	Wang et al. ²⁰
LC	Isotropic elastic	Elastic modulus = 0.3 MPa Poisson's ratio = 0.49	Sigal et al. ⁴⁵
Optic nerve (including pia)	Yeoh model	c1 = 0.088 MPa c2 = 0.482 MPa	This study
Border tissue	Yeoh model	c1 = 0.1707 MPa c2 = 4.2109 MPa c3 = -4.9742 MPa	Wang et al. ²⁰

* Collagen fibers in the scleral fiber ring were aligned circumferentially around scleral canal; fibers in other parts of the sclera were organized randomly.

average biomechanical properties as obtained experimentally from uniaxial tensile testing of the BMCC in this study. The sclera was modeled as a fiber-reinforced hyperelastic tissue, in which a scleral fiber ring (scleral flange) with a thickness of 0.45 mm was included (Fig. 4) to account for the circumferential alignment of collagen fibers around the scleral canal.²⁴ Collagen fibers in other scleral regions were considered randomly organized (in-plane isotropy). The choroid, LC, and neural tissues were modeled as isotropic hyperelastic materials; the dura was modeled as nonlinear hyperelastic materials. We also performed uniaxial tensile tests to assess the biomechanical properties of the ON, as it has been suggested that the ON contains abundant connective tissues and not just neural tissues.^{25,26} The average experimental data of 10 porcine ONs (that included the pia but excluded the dura) were obtained and fitted using a Yeoh model (see Supplementary Material for more details). For simplicity, we then simulated the ON (including the pia) as a single homogeneous structure. Because there are no available data in the literature regarding the biomechanical properties of the border tissues of Jacoby and Elschnig, their biomechanical properties were taken to be the same as those of the pia mater in a previous study,²⁰ as both border tissues are thought to be an extension of the pia. All biomechanical parameters/models used in this study are listed in Table 1.

Loading and Boundary Conditions. As IOP is a primary mechanical load that affects ocular structures and the primary risk factor for the development of glaucoma, we investigated the structural role of BM under an elevated IOP. To this end, an IOP of 15 mm Hg, and then 50 mm Hg, were applied to the inner limiting membrane in both models. The rectus muscle insertion regions of the globe were fixed and so was the optic nerve at the orbital apex region (Fig. 4, arrows).

Varying the Stiffness of BM. In our baseline model, the biomechanical properties of BM were assumed to be the same as those obtained for BMCC experimentally. However, such an approach may underestimate the actual stiffness of BM. To investigate the effects of BM stiffness on ONH deformations, we modified BM biomechanical properties (c1 and c2) to 1, 4, 7, 10, and 13.5 times the averaged experimental values

obtained from uniaxial testing for BMCC. This range of stiffness variation was calculated through a rule of mixture based on our own experimental data and data from the literature,^{14,23,27} as described in detail in Supplementary Material.

Output Measurement. We reported the mean effective strains in the LC and prelaminar tissues (Fig. 4B) in both models (and for both IOP levels). Effective strain is a single index that conveniently summarizes the three-dimensional (3D) state of deformations at a local tissue location and that takes into account both compressive and tensile effects. In this paper, the effective strain was defined as follows:

$$E' = E - \left(\frac{\text{tr}E}{3}\right)I \quad (1)$$

$$\text{Effective strain} = \sqrt{\frac{3}{2}E' : E'} \quad (2)$$

where E is the Green-Lagrange strain tensor and I is the second-order identity tensor.

RESULTS

Biomechanical Properties of BMCC

We found that BMCC exhibited a typical nonlinear stress/stretch behavior. BMCC stress-stretch curves are plotted in Figure 5. Individual stress-stretch curves were fitted with a Yeoh model and the extracted biomechanical properties are listed in Table 2. We additionally included the mean BM stress-stretch curve (Fig. 5B, bold black), which was obtained by taking the mean of all Yeoh parameters (c1 and c2) from all specimens. The average BMCC elastic (tangent) moduli (derived from the mean BMCC stress-stretch curve) for 0% and 5% strain were 1.60 ± 0.81 and 2.44 ± 1.02 MPa, respectively. Note that the tangent modulus at 0 strain roughly represents the tissue stiffness at the initial loading stage with a very low stress/strain level.

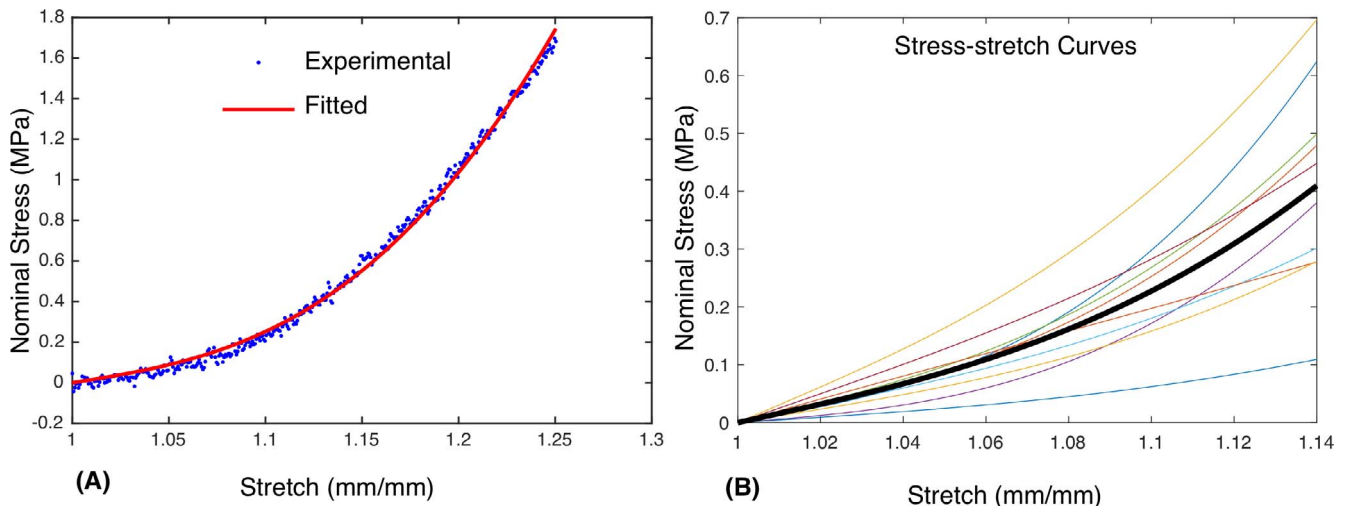


FIGURE 5. Uniaxial tensile test results of porcine BM-choroid samples. (A) Example shows the stress-stretch data obtained from uniaxial tensile testing that were fitted to a Yeoh model. (B) Fitting results of 10 BM-choroid complexes samples from 10 porcine eyes. The averaged stress-stretch response was indicated by the *black line in bold*.

Rupture Pressure of BMCC

Using 20 porcine eyes, we found that the average pressure required to induce mechanical failure of BMCC was 82 mm Hg (with an SD of 29 mm Hg; range, 39 to 147 mm Hg). All rupture pressure measurements are shown in a boxplot in Figure 6.

FE Modeling Predicts That BM Has an Influence on the Biomechanical Behavior of the ONH at an Elevated IOP Level

For an IOP of 50 mm Hg, BM stiffness had a significant effect on prelamina effective strains but not on the LC. Specifically, stiffer BMs increased the mean effective strains in the prelamina tissues (by 10.5%) but decreased them in the LC (by 0.7%), although this latter effect was relatively small.

For an IOP of 15 mm Hg, the effect of increasing BM stiffness on prelamina strain was still present but was smaller (2% increase in prelamina strain). This effect was negligible on LC strain (2% decrease). The LC and prelamina effective strains (as functions of the BM stiffening ratio for both IOP levels) and strain color maps in the ONH tissues (for an IOP of 50 mm Hg) are shown in Figure 7.

TABLE 2. Extracted Material Parameters for 10 Porcine Samples

Sample Number	c1 (MPa)	c2 (MPa)
1	0.22	5.77
2	0.26	3.59
3	0.51	3.94
4	0.10	3.86
5	0.29	3.55
6	0.25	1.50
7	0.42	1.71
8	0.08	0.65
9	0.35	0.27
10	0.19	1.68
Mean*	0.27	2.65
SD	0.14	1.74

* For the Yeoh model, average material parameters (c1 and c2) are equal to the parameters obtained from curve fitting of the average stress-stretch curves.

Finally, in the baseline model (for an IOP of 50 mm Hg), the distance between the center of the anterior LC surface and the plane of the BM opening (BMO) decreased by 0.5%, suggesting a slight anterior LC movement with increasing IOP. The scleral canal size also increased by 1.6%.

DISCUSSION

In this paper, we investigated the biomechanical properties of BMCC experimentally. We then evaluated the BM influence (computationally) on the deformations of the ONH following an acute elevation of IOP to 50 mm Hg. We found that the BMCC stiffness was high compared with other ocular tissues and that it could sustain a substantially high IOP without rupturing. Additionally, our models suggested that BM stiffness had a nonnegligible influence on IOP-induced ONH tissue deformations.

In ocular biomechanics, the biomechanics of BM has been given very little attention. To the best of our knowledge, only two peer-reviewed study reported values for the elastic modulus of BMCC using human samples. However, the study by Ugarte et al. defined the elastic modulus of BM as a strain to

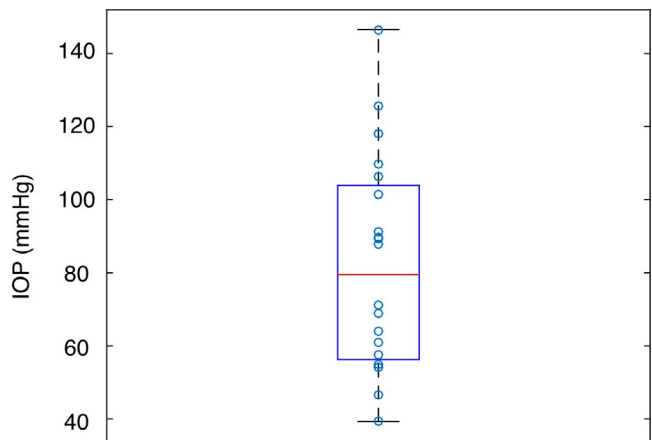


FIGURE 6. Boxplot of the burst test results. A scatter plot of all data points was overlaid on the boxplot to provide additional insights into the results.

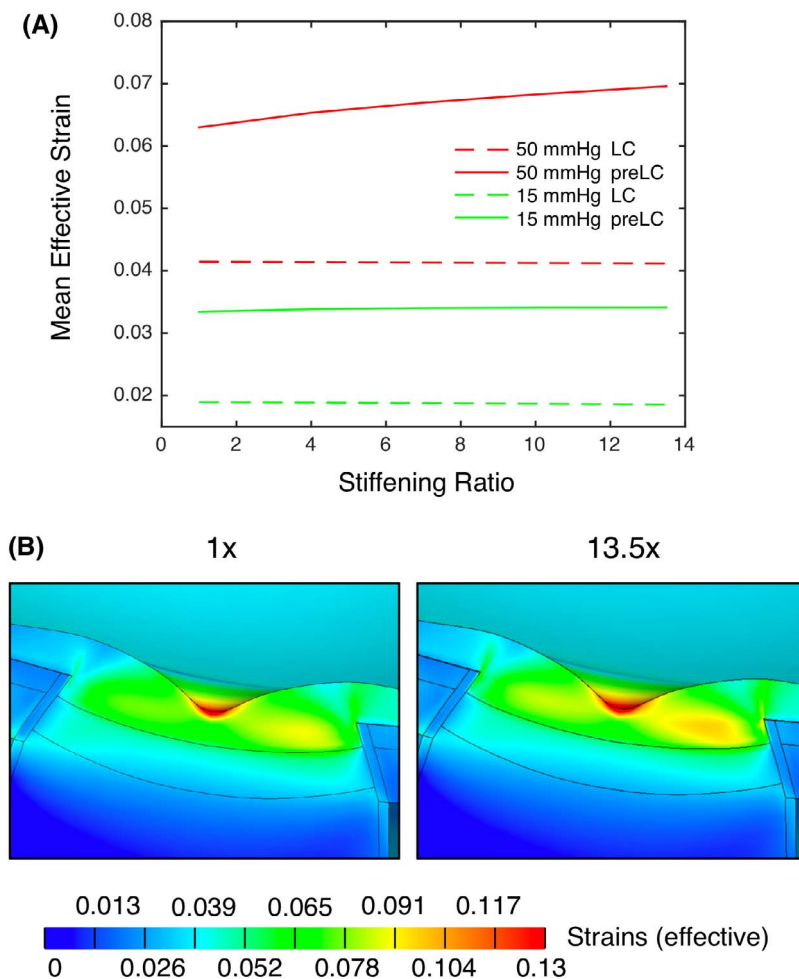


FIGURE 7. (A) Mean prelaminar (preLC) and LC strains as functions of BM stiffness (for IOPs of 15 and 50 mm Hg). (B) Effective strain distributions in the ONH for two models with different BM stiffnesses. Here, an IOP of 50 mm Hg was applied to the inner limiting membrane in both models. Higher strains were observed in the prelaminar when BM was stiffer. Stiffening ratio = (BM stiffness)/(BMCC stiffness measured experimentally).

stress ratio with units in mm/Pa.¹³ Therefore, little can be concluded from this study alone about the elastic modulus of BMCC. In our study, we found that BMCC of porcine eyes was a nonlinear soft tissue (stiffer with stretch) similar to other collagenous tissues such as the dura²⁰ or peripapillary sclera.²⁸ Our uniaxial tensile experiments showed that the average elastic moduli of BMCC at 0% and 5% strain were 1.60 ± 0.81 and 2.44 ± 1.02 MPa, respectively. For porcine eyes, the elastic moduli of BMCC samples in this study were found to be comparable or higher than those for the sclera (0.2 to 0.5 MPa for IOP of approximately 15 mm Hg^{29,30}; 7.96 ± 1.00 MPa at 8% strain³¹), for the cornea (0.1 to 0.5 MPa³²⁻³⁴), for the retina (0.011 MPa³⁵), and for the iris (0.004 MPa³⁶). As the specimen thicknesses in this study were much smaller than previous studies (less choroid included), the material parameters obtained here may be closer to that of the BM compared with previous studies.

Our burst tests showed that, on average, the BMCC alone was able to sustain an IOP of about 82 mm Hg without rupturing. Because the retina is extremely weak (elastic modulus = 0.011 MPa³⁵), it is most likely that the applied IOP was mainly borne by BMCC. It is interesting to note that each BMCC specimen exhibited significant deformations before its point of rupture (observed as considerable bulging in the pressure experiments; Fig. 3B). Following each rupture

test, we dissected each eye and found that there was no detachment of BM around the ora serrata and the scleral canal at the time of rupture. Histology also confirmed that BM remained attached in the ora serrata and the optic disc regions (Figs. 3D, 3E). This indicates that BM may exhibit good extensibility behavior under acute elevations of IOP.

Although BM may be stiff, its contribution to IOP resistance may be limited because of its small thickness ($5 \mu\text{m}^{23}$). Our FE analysis showed that its structural role was significant at an IOP of 50 mm Hg, especially its influence on the prelaminar tissue deformations. Specifically, our simulations predicted that IOP-induced prelaminar strains increased by 10.5% for BM stiffness increasing from 1 to 13.5 times that of BMCC. For a smaller IOP (i.e., 15 mm Hg), the effect of BM stiffness on prelaminar strain was still present but was smaller (2% increase in prelaminar strain for BM stiffness increasing from 1 to 13.5 times that of BMCC). Overall, our data suggest that BM stiffness may alter the biomechanical environment of the ONH but only at elevated levels of IOP.

On the contrary, increasing the stiffness of BM had almost no impact on LC strains, and this was true at any IOP level (15 or 50 mm Hg). A previous study found that absence of peripapillary BM in peripapillary atrophy was associated with slower visual field progression in glaucoma.¹⁰ The authors speculated that the absence of BM in peripapillary atrophy may

be able to reduce the LC stress. However, their speculation was not supported by this study, in which we found a slightly higher LC strain (thus a higher LC stress) in the model with a softer BM. Interestingly, we found a smaller prelaminar strain in the model with a softer BM, which might be able to explain the slow progression of visual field in glaucoma with absence of peripapillary BM.

In view of the relatively high rupture pressure of BMCC keeping the IOP up to a level of about 80 mm Hg, one may consider the BMCC being the second strongest tissue in the eye second only to the corneoscleral shell. This example alone may show the potential biomechanical importance of BM in the structural stiffness of the eye. This notion is in agreement with the clinical observation that non-axially elongated eyes can show scleral staphylomata in regions in which BM developed a defect due to a toxoplasmatic retinochoroidal inflammation.³⁷ However, we do not exclude the fact that the sclera can also be damaged by inflammation, which could also yield staphyloma. The result of a relatively high rupture pressure of BMCC might have been unexpected because until now, BM has mostly been assigned to a role in separating the retinal tissue from the choroidal space. Based on the biomechanical findings in this study one may also discuss whether the noncompressible BM, when theoretically elongating in the midperipheral region of the fundus and thus extending backward, could lead to a compression and thinning of the choroid and a secondary elongation of the sclera most markedly at the posterior pole. Such a mechanism has recently been discussed to be involved in the process of emmetropization and myopization.¹² The biomechanical properties of BM may also be of importance to explain the development of macular BM defects in axially highly myopic eyes.³⁸ Because BM is stiff and sandwiched by soft tissues (i.e., retina and choroid), it might serve as a connector which is able to transmit displacements/forces between the anterior segment and the posterior segment of the eye. For example, it has been shown that, during accommodation, the ciliary muscle contracted and moved forward, which pulled the choroid, retina and BM anteriorly (relative to the sclera). The displacements of retina, choroid, and BM were substantial and presented in a large region that extend up to 4 to 7 mm posterior to ora serrata in rhesus monkey eyes.³⁹ It has been speculated that BM forces (originating in the anterior portion of the eye) could be transmitted to the ONH and affect functions and structures of ONH tissues.⁴⁰ However, this hypothesis remains to be proven.

Limitations

In this study, several limitations warrant further discussion. First, the biomechanical properties and rupture pressures of BMCC were experimentally measured using porcine tissues and thus may not be representative of human eyes. This work should be repeated using fresh human donor eyes.

Second, the specimens in the uniaxial test were BMCC. Although we were more interested in understanding the BM stiffness and its structural role in the eye, we were unable to isolate the BM alone without destroying its structural integrity. In the uniaxial test, we removed the choroid as much as possible from the specimens. The average thickness of our specimens was $21 \pm 4.9 \mu\text{m}$, which is much thinner than those of the previous two studies (80^{14} and $\sim 130 \mu\text{m}^{13}$). The thin samples used in this study may provide a hint on the BM material properties. Moreover, we used a microscope to assess the mechanical integrity of all BMCC specimens, which may not be able to detect damages of the samples at the microscopic level. However, if such damages were to occur,

it is unlikely that the specimen would have been able to resist high stresses during uniaxial tensile testing.

Third, our burst tests measured the ultimate IOP before BMCC rupture. Our tests showed that the structural strength of BMCC was not negligible. In other words, BMCC may not yet be a fragile membrane and may have a role to play in glaucoma, myopia, AMD, and peripapillary atrophy. However, please do note that we do not yet know if the adherent vitreous gel would have had an impact during these experiments, and further experiments that liquefy the vitreous prior testing should be warranted. Our reported burst pressures were also highly variable across specimen, and it is not yet known why. Please also note that our experimental protocols during our burst tests could be adapted to better assess the biomechanical properties of BMCC under physiologic loading, and this should be considered in future BMCC studies.

Fourth, BM was considered isotropic (with no specific collagen orientation) in all FE simulations. It is not yet known as to whether BM exhibits a collagenous ring immediately adjacent to the optic disc (as is true for the sclera²⁴). Further microstructure experiments on Bruch's membrane will be needed as this may improve the quality of our models.

Fifth, in the FE simulations, we assumed that the biomechanical properties of the border tissues of Jacoby and Elschnig were identical to those of the pia and dura. This assumption may not be correct, as collagen fiber organization in the border tissues could be significantly different from that in the pia due to different loading environments (e.g., the pia is exposed to the cerebrospinal fluid pressure while the border tissues are not). Future studies are needed to investigate the border tissue properties and how they could influence the biomechanics of the ONH. Furthermore, we assumed the scleral isotropy/anisotropy in various regions based on collagen fiber distributions without considering other structural proteins such as elastin. Future models may need to consider the distributions of elastin and other constituents.⁴¹ In addition, in the baseline model, the biomechanical properties for BMCC were also used for BM. This may be an underestimation. Because our BMCC elastic moduli were higher than those reported in the literature for the choroid (between 0.2 and 0.7 MPa¹⁴), and because BM is considerably thinner than the choroid, it would be plausible for the elastic modulus of BM to be considerably higher than that of the choroid or that of BMCC. Using a rule of mixture, we estimated the elastic modulus of BM (at 0% strain) to be between 2.7 and 21.6 MPa, but it is important to emphasize that this is only an estimate and not a direct experimental characterization. We also used this range of stiffness to better understand the effects of BM stiffness on ONH deformations. In addition, we modeled BM with a one-element layer to avoid extremely low-quality elements. As the dimension of BM along the thickness direction is much smaller than along the other two perpendicular directions, increasing the number of elements along the thickness direction could reduce the element quality dramatically. Typically, for such extremely thin structures, shell elements with adequate element equations are preferred. To this end, we constructed a new model in which BM was simulated with four-noded shell elements (see Supplementary Material for more details). We found that the difference in strain between the two modeling approaches (shell elements versus hexahedral elements) was less than 1.2%. This suggests that using a one-element layer approach (with hexahedral elements) is acceptable to model BM.

Sixth, we used a constant scleral thickness for the entire globe, but the sclera is known to exhibit large thickness variations.⁴² However, because we took into account scleral thickness variations in the region immediately adjacent to the disc (i.e., scleral flange), the assumption of a constant globe

thickness should not have an impact on any trends we are reporting. However, it is possible that strain magnitudes would be slightly affected if we were to use a nonconstant scleral thickness for the entire globe. Future studies may consider using a higher fidelity model with a more realistic eye geometry to better simulate the eye.

Seventh, tissue shrinkage is typical for any histologic processing⁴³ and is likely to have occurred in our study. However, because our OCT thickness measurements of BMCC (average: 21 μm) were in close agreement with those obtained from histology (average: 20.3 μm), tissue shrinkage along the thickness direction may have been minimal. Furthermore, it should be emphasized that histology was mostly performed to ensure that we biomechanically tested the right tissues and to ensure that BM did not detach from the ora serrata or the optic disc during the burst tests. Finally, we estimated BMCC biomechanical properties using tissue thickness measured from OCT (and not from histology), so that tissue shrinkage did not affect our modeling predictions.

In conclusion, we found that BMCC has a high material stiffness. Furthermore, BMCC can sustain a substantially high IOP before rupture. Additionally, BM may have a nonnegligible influence on IOP-induced ONH deformations. The potential roles of BM in peripapillary atrophy, glaucoma, and myopia need to be investigated in future studies.

Acknowledgments

The authors thank Ko Zhen Yu Gordon and Tin A. Tun for helping with the OCT imaging.

Supported by National University of Singapore Young Investigator Award NUSYIA_FY13_P03, R-397-000-174-133 (MJAG) and Tier 2 Grant R-397-000-280-112 (Ministry of Education, Singapore).

Disclosure: **X. Wang**, None; **C.K.G. Teoh**, None; **A.S.Y. Chan**, None; **S. Thangarajoo**, None; **J.B. Jonas**, Mundipharma Co. (C), P; **M.J.A. Girard**, None

References

- Booij JC, Baas DC, Beisekeeva J, et al. The dynamic nature of Bruch's membrane. *Prog Retinal Eye Res.* 2010;29:1-18.
- van Lookeren Campagne M, LeCouter J, Yaspan BL, Ye W. Mechanisms of age-related macular degeneration and therapeutic opportunities. *J Pathol.* 2014;232:151-164.
- Jonas JB, Wang YX, Zhang Q, et al. Parapapillary gamma zone and axial elongation-associated optic disc rotation: the Beijing Eye Study. *Invest Ophthalmol Vis Sci.* 2016;57:396-402.
- Jonas JB, Jonas SB, Jonas RA, et al. Parapapillary atrophy: histological gamma zone and delta zone. *PLoS One.* 2012;7:e47237.
- Wang YX, Jiang R, Wang NL, et al. Acute peripapillary retinal pigment epithelium changes associated with acute intraocular pressure elevation. *Ophthalmology.* 2015;122:2022-2028.
- Panda-Jonas S, Xu L, Yang H, et al. Optic nerve head morphology in young patients after antiglaucomatous filtering surgery. *Acta Ophthalmol.* 2014;92:59-64.
- Hayreh SS, Jonas JB, Zimmerman MB. Parapapillary chorioretinal atrophy in chronic high-pressure experimental glaucoma in rhesus monkeys. *Invest Ophthalmol Vis Sci.* 1998;39:2296-2303.
- Wang X, Beotra MR, Tun TA, et al. In vivo 3-dimensional strain mapping confirms large optic nerve head deformations following horizontal eye movements. *Invest Ophthalmol Vis Sci.* 2016;57:5825-5833.
- Wang X, Fisher LK, Milea D, et al. Predictions of optic nerve traction forces and peripapillary tissue stresses following horizontal eye movements. *Invest Ophthalmol Vis Sci.* 2017;58:2044-2053.
- Yamada H, Akagi T, Nakanishi H, et al. Microstructure of peripapillary atrophy and subsequent visual field progression in treated primary open-angle glaucoma. *Ophthalmology.* 2016;123:542-551.
- Fan Y, Jonas J, Wang Y, et al. Horizontal and vertical optic disc rotation. The Beijing Eye Study. *PLoS One.* 2017;12:e0175749.
- Jonas JB, Ohno-Matsui K, Jiang WJ, Panda-Jonas S. Bruch membrane and the mechanism of myopization: a new theory. *Retina.* 2017;37:1428-1440.
- Ugarte M, Hussain AA, Marshall J. An experimental study of the elastic properties of the human Bruch's membrane-choroid complex: relevance to ageing. *Br J Ophthalmol.* 2006;90:621-626.
- Friberg TR, Lace JW. A comparison of the elastic properties of human choroid and sclera. *Exp Eye Res.* 1988;47:429-436.
- Girard M, Suh JKF, Hart RT, et al. Effects of storage time on the mechanical properties of rabbit peripapillary sclera after enucleation. *Curr Eye Res.* 2007;32:465-470.
- Munoz MJ, Bea JA, Rodriguez JF, et al. An experimental study of the mouse skin behaviour: damage and inelastic aspects. *J Biomech.* 2008;41:93-99.
- O'Hagan JJ, Samani A. Measurement of the hyperelastic properties of 44 pathological ex vivo breast tissue samples. *Physics Med Biol.* 2009;54:2557-2569.
- Hollows FC, Graham PA. Intra-ocular pressure, glaucoma, and glaucoma suspects in a defined population. *Br J Ophthalmol.* 1966;50:570-586.
- Chew AC, Chan A, Nongpiur ME, et al. A rabbit model study to determine the efficacy of a prototype corneal endothelium protector during cataract surgery. *J Ophthalmol.* 2017;2017:6906139.
- Wang X, Rumpel H, Lim WEH, et al. Finite element analysis predicts large optic nerve head strains during horizontal eye movements. *Invest Ophthalmol Vis Sci.* 2016;57:2452-2462.
- Jonas JB, Holbach L, Panda-Jonas S. Peripapillary ring: histology and correlations. *Acta Ophthalmol.* 2014;92:e273-e279.
- Jiang R, Wang YX, Wei WB, et al. Peripapillary choroidal thickness in adult chinese: The Beijing Eye Study. *Invest Ophthalmol Vis Sci.* 2015;56:4045-4052.
- Jonas JB, Holbach L, Panda-Jonas S. Bruch's membrane thickness in high myopia. *Acta Ophthalmol.* 2014;92:e470-e474.
- Zhang L, Albon J, Jones H, et al. Collagen microstructural factors influencing optic nerve head biomechanics. *Invest Ophthalmol Vis Sci.* 2015;56:2031-2042.
- Jeffery G, Evans A, Albon J, et al. The human optic nerve: fascicular organisation and connective tissue types along the extra-fascicular matrix. *Anatomy Embryol.* 1995;191:491-502.
- Shin A, Yoo L, Park J, Demer JL. Finite element biomechanics of optic nerve sheath traction in adduction. *J Biomech Eng.* 2017;139:101010.
- Bai HX, Mao Y, Shen L, et al. Bruch's membrane thickness in relationship to axial length. *PLoS One.* 2017;12:e0182080.
- Girard MJA, Downs JC, Bottlang M, et al. Peripapillary and posterior scleral mechanics—part ii: experimental and inverse finite element characterization. *J Biomech Eng.* 2009;131:051012.
- Pierscionek BK, Asejczyk-Widlicka M, Schachar RA. The effect of changing intraocular pressure on the corneal and scleral curvatures in the fresh porcine eye. *Br J Ophthalmol.* 2007;91:801-803.
- Leung LKK, Ko MWL, Ye C, et al. Noninvasive measurement of scleral stiffness and tangent modulus in porcine eyes. *Invest Ophthalmol Vis Sci.* 2014;55:3721-3726.

31. Liu TX, Wang Z. Collagen crosslinking of porcine sclera using genipin. *Acta Ophthalmol.* 2013;91:e253-e257.
32. Ko MW, Leung LK, Lam DC, Leung CK. Characterization of corneal tangent modulus in vivo. *Acta Ophthalmol.* 2013;91:e263-e269.
33. Elsheikh A, Alhasso D, Rama P. Biomechanical properties of human and porcine corneas. *Exp Eye Res.* 2008;86:783-790.
34. Liu J, He X. Corneal stiffness affects IOP elevation during rapid volume change in the eye. *Invest Ophthalmol Vis Sci.* 2009;50:2224-2229.
35. Worthington KS, Wiley LA, Bartlett AM, et al. Mechanical properties of murine and porcine ocular tissues in compression. *Exp Eye Res.* 2014;121:194-199.
36. Whitcomb JE, Barnett VA, Olsen TW, Barocas VH. Ex vivo porcine iris stiffening due to drug stimulation. *Exp Eye Res.* 2009;89:456-461.
37. Jonas JB, Panda-Jonas S. Secondary Bruch's membrane defects and scleral staphyloma in toxoplasmosis. *Acta Ophthalmol.* 2016;94:e664-e666.
38. Jonas JB, Ohno-Matsui K, Spaide RF, et al. Macular bruch's membrane defects and axial length: association with gamma zone and delta zone in peripapillary region. *Invest Ophthalmol Vis Sci.* 2013;54:1295-1302.
39. Croft MA, Nork TM, McDonald JP, et al. Accommodative movements of the vitreous membrane, choroid, and sclera in young and presbyopic human and nonhuman primate eyes. *Invest Ophthalmol Vis Sci.* 2013;54:5049-5058.
40. Croft MA, Lutjen-Drecoll E, Kaufman PL. Age-related posterior ciliary muscle restriction: a link between trabecular meshwork and optic nerve head pathophysiology. *Exp Eye Res.* 2017;158:187-189.
41. Quigley HA, Brown A, Dorman-Pease ME. Alterations in elastin of the optic nerve head in human and experimental glaucoma. *Br J Ophthalmol.* 1991;75:552-557.
42. Norman RE, Flanagan JG, Rausch SM, et al. Dimensions of the human sclera: thickness measurement and regional changes with axial length. *Exp Eye Res.* 2010;90:277-284.
43. Tran H, Jan NJ, Hu D, et al. Formalin fixation and cryosectioning cause only minimal changes in shape or size of ocular tissues. *Sci Rep.* 2017;7:12065.
44. Girard MJA, Suh JKF, Bottlang M, et al. Scleral biomechanics in the aging monkey eye. *Invest Ophthalmol Vis Sci.* 2009;50:5226-5237.
45. Sigal IA, Flanagan JG, Tertinegg I, Ethier CR. Modeling individual-specific human optic nerve head biomechanics. Part II: influence of material properties. *Biomech Model Mechanobiol.* 2009;8:99-109.